Soil moisture modulation of midlatitude heat waves

Adam Michael Bauer* (Department of Physics, University of Illinois at Urbana Champaign, Loomis Laboratory, Urbana, IL; adammb4 [at] illinois [dot] edu)

Lucas R. Vargas Zeppetello (Department of Earth and Planetary Sciences, Harvard University, Cambridge, MA; lzeppetello [at] fas [dot] harvard [dot] edu)

Cristian Proistosescu (Department of Atmospheric Sciences & Department of Geology, University of Illinois at Urbana Champaign, Urbana IL; cristi [at] illinois [dot] edu)

The following is a non-peer reviewed preprint submitted to EarthArXiv. It should not be cited in any other works.

This manuscript is in review for publication in Nature Geoscience. Updates to the preprint will be done as necessary and in accordance with the journal's review rules and guidelines.

Soil moisture modulation of midlatitude heat waves

Adam Michael Bauer[1*], Lucas R. Vargas Zeppetello[2†] and Cristian Proistosescu[3,4†]

[1]Department of Physics, University of Illinois at Urbana Champaign, Loomis Laboratory, Urbana, IL, USA.
[2]Department of Earth and Planetary Sciences, Harvard University, Cambridge, MA, USA.
[3]Department of Atmospheric Sciences, University of Illinois at Urbana Champaign, Urbana, IL, USA.
[4]Department of Geology, University of Illinois at Urbana Champaign, Urbana, IL, USA.

*Corresponding author(s). E-mail(s): adammb4@illinois.edu;
Contributing authors: lzeppetello@fas.harvard.edu; cristi@illinois.edu;
†These authors contributed equally to this work.

Abstract

Heat waves are broadly expected to increase in severity and frequency under climate change. Case studies highlight a number of physical mechanisms that play a role in present-day heat waves, which typically occur during a coalescence of anomalous atmospheric and land surface conditions. However, a unified model of heat wave physics is lacking, primarily owing to difficulty in disentangling the forcing versus feedback roles of soil moisture and atmospheric variability. Here, we provide observational evidence that soil moisture modulation of heat waves is a generic feature of midlatitude continental climates, and develop a theoretical framework to understand this modulation. Using separation of timescales we derive a diagnostic equation for the nonlinear response of temperature to soil moisture variations, and a dynamical Hasselmann-like model for the soil moisture variations themselves. We find that soil moisture fluctuations control the frequency and intensity of temperature extremes by slowly altering the background state on which rapid atmospheric variability acts, rather than by altering atmospheric variability itself. We also find the slow soil moisture variations are well-approximated as being primarily driven by stochastic precipitation variability. Our framework provides a first-principles understanding of soil moisture's role in midlatitude temperature extremes.

Keywords: heat waves, soil moisture, climate extremes, stochastic models

Heat waves inflict immense damage to economies [1], ecosystems [2], and human health [3]; the European heat wave of 2003 alone is estimated to have killed over seventy thousand people. As average temperatures increase, mean shifts of daily temperature distributions inexorably lead to increased frequency and severity of heat waves [4, 5]. The precise impact of a warming climate on extreme events, however, is highly sensitive to the details of the underlying distribution [6]. A short and nonstationary observational record makes it difficult to robustly estimate how often a given historical temperature threshold should be exceeded. Statistical approaches to attribution depend on fitting the limited number of observations to a generalized probability distribution with many free parameters, which makes it difficult to assign a likelihood to even well-characterized events such as the 2021 Pacific Northwest Heat Wave [7]. At the same time, climate models show no consistent pattern between mean warming and changes in temperature distributions [8], and are biased in their representation of temperature variability [9]. These limitations of both the empirical record and numerical models highlight a growing need for a general theory of present-day heat waves, especially outside the tropics [10, 11].

A unified understanding of heat waves has been hampered by difficulty in disentangling contributing mechanisms that act across a breadth of timescales: atmospheric blocking [12], cloud variability [13], and thermal advection near the surface [14, 15] contribute to fast variations in near-surface temperature relative to soil moisture dynamics [16–20]. Throughout this paper, we will refer to the relatively fast processes (variations in blocking, thermal advection, and cloud radiative effects) as the atmospheric forcing in contrast to variations driven by (comparatively) slower fluctuations in soil moisture. Capturing the interaction of these mechanisms is a key component of any physical theory of heat waves, as it is a general property of stochastic systems that the shape of distributional tails is controlled by the interaction of mechanisms across timescales [21].

A generic picture of how atmospheric circulation contributes to generating a midlatitude summer "heat dome" involves the spatial stagnation of a high pressure system, known as a "blocking" event. Anticyclonic circulation leads to enhanced surface warming through a combination of subsidence-driven adiabatic heating [12], advection of warm tropical air [22], and suppression of convection and clouds [23]. Each of these mechanisms leads to increased energetic forcing of the surface boundary layer, and thus, of the surface.

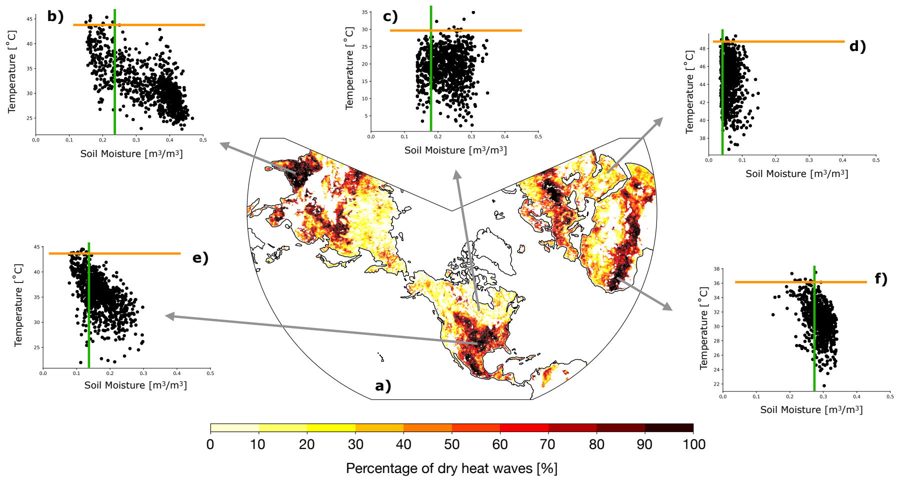

Fig. 1 Dry heat waves. a) shows the percentage of days where the maximum temperature exceeds the local 99$^{\text{th}}$ percentile while soil moisture is less than the local first quantile. **b) – f)** show daily maximum temperature-soil moisture phase space plots with the horizontal orange line indicating the local 99$^{\text{th}}$ temperature percentile and the vertical green line indicating the local first soil moisture quantile.

While this excess of energy inevitably warms the surface, it does not necessarily lead to the onset of a heat wave. Instead, the extent to which increased surface forcing leads to extreme temperatures is modulated by the thermodynamic state of the surface. The land surface thermodynamic state controls the partitioning of incoming atmospheric forcing into two channels: an ET channel, where incoming energy evaporates moisture, and a heating channel, where incoming energy raises temperatures. The distraction of energy by ET away from heating the surface is commonly referred to as "latent cooling." The strength of latent cooling is controlled by two factors: (1) the atmospheric vapor pressure deficit (VPD) and (2) the available moisture in the soil for ET [24–26]. The influence of soil moisture on individual heat waves has been shown in a number of case studies [27]. However, a theoretical model of this influence is lacking, as is quantification of its generality without using climate model or reanalysis output.

Soil moisture modulation of heat wave frequency

Here, we quantitatively describe how each of the contributing factors to temperature extremes – atmospheric forcing and soil moisture variability – influence the intensity and frequency of heat waves. We begin by using observational data to show the generality of soil moisture's influence on heat waves in midlatitude climates. To our knowledge, this is the first demonstration of soil moisture's general influence on heat waves using observational data in the literature. We then use a much longer reanalysis product to demonstrate the fast-slow influence of atmospheric forcing and soil moisture dynamics on temperature distributions, as well as statistically quantify the impact of soil moisture on near-surface temperature. We interpret these data by building a conceptual model that quantifies the impact of soil moisture on the intensity and frequency of temperature extremes. We do this by first quantifying how a soil moisture anomaly modifies the probability of a heat wave occurring under favorable atmospheric forcing, and then quantifying the frequency of soil moisture anomalies.

Observations in Figure 1a show a clear connection between extremely hot days and soil moisture deficits in the midlatitudes. In many regions, more than 90% of days where temperatures exceed the local 99$^{\text{th}}$ percentile occur when the soil is dry (see *Methods*). The influence is strongest in continental midlatitude regions such as the central United States and central Europe, as well as subtropical regions with strong precipitation seasonality such as South Asia and the Sahel. The influence is weakest in high latitudes regions such as Canada and Siberia, and in very arid regions such as the US Southwest and the Sahara.

The difference between areas where soil moisture's influence is sizable and areas where its influence is moderate to minimal is best visualized in temperature-soil moisture phase space (Figs. 1b–f). In regions where extremely high temperatures are clustered around periods where the soil is dry, a nonlinear relationship emerges where soil moisture depletion leads to a rapid upward shift in temperature.

To understand this relationship, we focus on a small number of continental locations in the United States that span the potential influence of soil moisture on near-surface temperature (see Table 2) and use the ERA5 reanalysis product that provides a longer record of surface temperature and soil moisture (see *Methods* for details) [28]. The reanalysis record shows the same emergent relationship between temperature and soil moisture (Fig. 2A–C) found in observations, but provides a long enough record to allow us to estimate conditional means and probability distribution functions of temperature for individual soil moisture quantiles (Fig. 2A–I). We find that soil moisture has a potentially large impact on mean temperature across soil moisture quantiles (up to $\sim 5 - 10$ °C), but has a minimal impact on temperature variability within each quantile regardless of its impact on mean temperature (see Fig. 2G—L).

Based on our analysis in Figures 1 and 2, we highlight two conclusions that inform and motivate our theoretical model. The first is that soil moisture influences heat waves primarily by modulating the background state on top of which atmospheric variability acts, rather than by changing atmospheric variability itself. However, the static scatter-plot analysis carried out in Figs. 1 and 2 cannot answer the question of whether these soil moisture variations are themselves a response to – and thus a feedback on – synoptic forcing. We will explore this ambiguity below.

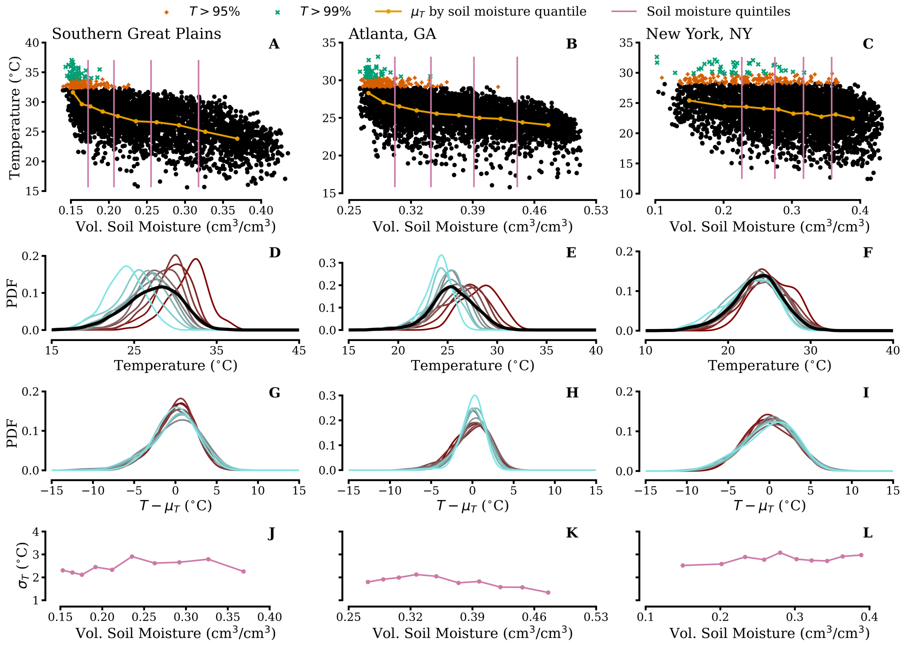

Fig. 2 Decoupling soil moisture and atmospheric variability. A–C shows scatter plots of the temperature-soil moisture phase space for three locations, with extreme temperature days colored orange ($T > 95^{\text{th}}$ percentile) and green ($T > 99^{\text{th}}$), as well as the mean temperature averaged within each soil moisture quantile (gold curve), see the legend above **A–C**. **D–F** show the estimated probability distribution function (PDF) of near surface temperature for a given quantile of soil moisture using ERA5 reanalysis output. The cyan (maroon, resp.) PDFs are for the high (low, resp.) quantiles of soil moisture. The mean PDF is in black. **G–I** are as **D–F**, after subtracting the mean. **J–L** show the standard deviation of the temperature PDF in each soil moisture quantile.

The second implication is that the degree to which soil moisture impacts heat wave frequency and intensity is related to the strength of the nonlinear correspondence between soil moisture and temperature. Indeed, soil moisture has a sizable impact in the SGP which has a strongly nonlinear relationship between soil moisture and temperature, whereas soil moisture has a minimal impact in New York which has a weak nonlinearity strength (see the gold lines in Fig. 2A—C). Atlanta serves as a “middle of the road” example between the SGP and New York.

Results

We now turn to building a conceptual *soil moisture—atmosphere coupled model* (SMACM) that will provide insight into both the nonlinear coupling of soil moisture and temperature, as well as the mechanisms that drive soil moisture variations. SMACM is formulated as a one-dimensional box model of surface temperature and soil moisture, where the land surface is forced by the atmosphere. A full derivation of model equations and our model evaluation is

Table 1 SMACM parameters. List of SMACM parameter names, their symbols, average order of magnitude (OM), and units.

Parameter	Symbol	OM	Units
Effective heat capacity of surface layer	C	10	J K^{-1} m^{-2}
Two meter air temperature	T	10^2	K
Time	t	1	s
Radiative forcing	$\mathcal{F}$	10^2	W m^{-2}
Dry feedback strength	α	10	W m^{-2} K^{-1}
Latent heat of vaporization	λ	10^6	J kg H_2O^{-1}
Surface evaporative conductance	ν	10^{-2}	kg H_2O m^{-2} s^{-1}
Clausius-Clapeyron derivative at mean T_d	γ	10^{-4}	K^{-1}
Soil moisture fraction	m	10^{-1}	–
Constant deep soil moisture fraction	m_0	10^{-1}	–
Two meter dew point temperature	T_d	10^2	K
Soil holding capacity	μ	10	kg H_2O m^{-2}
Precipitation	$\mathcal{P}$	10^{-1}	kg H_2O m^{-2} s^{-1}

provided in the *Methods*; see Table 1 for parameter descriptions, units, and average order of magnitudes used in this study.

Assuming the timescale of thermal adjustment is much smaller than that of moisture adjustment (we prove this explicitly in the *Methods*, but it is a common assumption in various studies, e.g., [18–20]) and using the governing equations of SMACM (Eqns. (12) and (13) in the *Methods*), a diagnostic relationship between temperature, T, and soil moisture, m, can be derived as

$$T(m) = T_0 \left(\frac{1}{1 + \eta m} \right) + T_d, \tag{1}$$

where we have defined $T_0 := \mathcal{F}/(\alpha + \lambda\nu\gamma m_0)$ and $\eta := \lambda\gamma\nu/(\alpha + \lambda\gamma\nu m_0)$. T_0 and η have salient physical interpretations. T_0 is the maximum soil moisture induced temperature departure from the dew point temperature (occurring when the surface is completely dry). η measures the coupling strength between soil moisture and temperature, and is determined by the relative strength of the latent heat feedback associated with a saturated *surface* layer to the strength of the dry feedback and the recalcitrant latent heat feedback associated with deep soil moisture.

This procedure separates the two aforementioned modes of temperature variability; the dew point temperature is a purely additive component to the soil moisture dependent piece. In the language of dynamical systems, (1) is referred to as a *nullcline*, defined as a curve in phase space where the dynamics of one or more variables is neglected [29, 30], and we will henceforth refer to (1) as the temperature nullcline, or just "the nullcline."

Heat wave frequency

The nullcline can be used to understand the role of soil moisture in heat wave frequency. In Figure 3A–C, we show the daily temperature-soil moisture

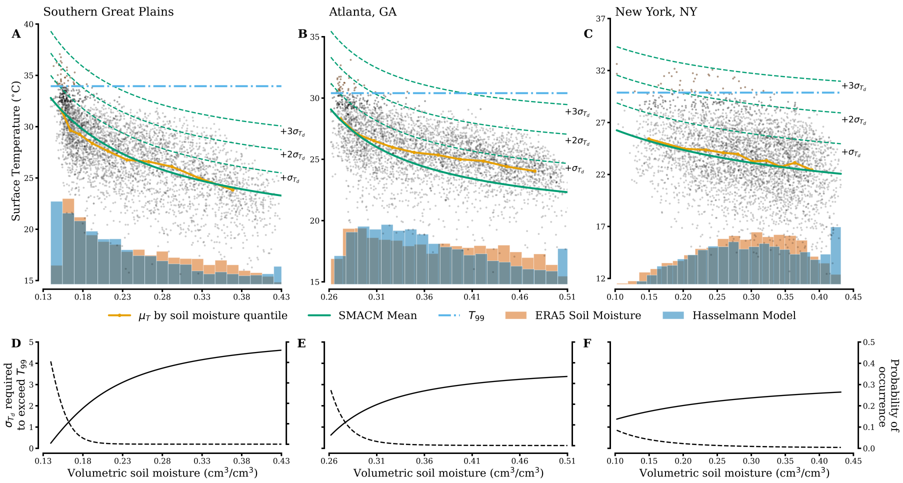

Fig. 3 Quantifying the impact of soil moisture on heat wave frequency and intensity. A–C shows the temperature-soil moisture phase space for the SGP, Atlanta and New York, respectively, with the mean temperature by soil moisture quantile (gold line) and the temperature nullcline (Eqn. (1), green solid line). The dashed lines are the nullcline after anomalies of varying size in two meter dew point temperature have been applied. We also show the soil moisture histograms for ERA5 (salmon) and our Hasselmann model (3) (light blue). In **D–F**, the solid lines show the required anomaly size in the two meter dew point temperature for two meter temperature given by (1) to exceed the 99^{th} percentile in each location as a function of soil moisture. The dashed lines represent the probability of such an anomaly to occur, assuming a normally distributed dew point temperature.

phase space of the SGP, Atlanta, and New York with the temperature nullcline overlaid in green, assuming mean values for the net shortwave radiation and dew point temperature. We apply dew point temperature anomalies to the nullcline in each location to show the impact of atmospheric variability on the orientation of the nullcline in phase space. (An analogous figure for radiative forcing anomalies is provided in the *Supplementary Information*.)

When the soil is dry, less extreme dew point temperature anomalies are needed to exceed the local 99^{th} temperature percentile than when the soil is wet. We calculate the anomaly size needed to exceed the local 99^{th} percentile, as well as the probability of such an event occurring, as a function of soil moisture in panel 3D–F. For the SGP, the anomaly size required grows nonlinearly with soil moisture, whereas in New York the anomaly size is relatively flat and linear, showing that the higher the degree of nonlinearity between temperature and soil moisture, the more dry soils load the dice in favor of heat waves.

This can be explained by the coupling parameter η determining the curvature of the nullcline, i.e.,

$$\Delta T := \frac{T(m=1) - T(m=0)}{T_0} = \frac{\eta}{\eta + 1}. \tag{2}$$

If η is small (weak coupling regime), then $\Delta T \sim 0$, and soil moisture's influence on temperature disappears by virtue of the nullcline "flattening out." If η is large (strong coupling regime), then $\Delta T \sim 1$, resulting in the maximum difference between temperatures when the soil is dry or wet.

This showcases how the nonlinear coupling between soil moisture and temperature influences heat wave frequency: in locations with high η parameters, relatively common atmospheric events can cause temperature extremes when the soil is dry, implying that the frequency at which the soil dries out is a leading order indicator of heat waves in these locations. In locations with low η parameters, soil moisture matters little for heat wave frequency, if at all.

Heat wave intensity

Soil moisture's impact on heat wave intensity can be determined by assuming the soil is dry (if the soil is wet, heat waves are either just as or far less likely than when the soil is dry, depending on the coupling strength, see Figure 3D–F). In this regime, the departure of temperature away from the dew point temperature is determined by T_0, or "dry-out" temperature. The dry-out temperature depends on root-level soil moisture content, highlighting the role of deep soil moisture content on surface temperatures. Atmospheric dynamics impact the nullcline by altering the magnitude of the dry-out temperature. (Recall T_0 linearly depends on $\mathcal{F}$.) Thus, when surface forcing is high, the impact of the land thermodynamics on near surface temperature is exacerbated, particularly when the soil is dry. Our framework therefore suggests an important feedback mechanism between the atmospheric forcing and local thermodynamics, where strong atmospheric forcing makes the land response more skewed towards extremely high temperatures. We find across a variety of nullcline configurations, T_0 captures at least 52% of the temperature departure from the mean dew point temperature on the hottest day in the reanalysis product (see Table 2).

Soil moisture variability

So far, we have consistently invoked dry soil conditions to demonstrate the role of soil moisture in temperature extremes. But how often does the soil dry out? Indeed, the nonlinearity between temperature and soil moisture described above is a necessary, but not sufficient condition for soil moisture dynamics being a leading order factor in heat wave frequency. Soil moisture is impacted by both precipitation frequency and intensity that ultimately control its influence on temperature. For example, if the temperature nullcline is highly nonlinear, but the soil is perpetually dry or wet, then the nonlinearity matters little because soil moisture is too restricted in phase space to cause significant temperature variance (panel 1D is an example of this scenario). Hence, the soil moisture distribution also plays a crucial role in assessing the amount of temperature variance owing to soil moisture.

Table 2 SMACM parameter value impacts on heat wave intensity and frequency. We calculate the ratio of temperature variance owing to soil moisture to total temperature variance for five locations in the continental United States. We also show the ratio of the dry-out temperature, T_0, to the maximum departure from the mean dew point temperature in the reanalysis product, $T_X := \max(T) - \bar{T}_d$, for five locations in the continental United States. Provided as well are the nonlinear strength parameter, η, the dry-out temperature, T_0, and the mean and variance of the soil moisture distribution in each location.

Location	η [–]	T_0 [°C]	$\overline{m}$ [–]	σ_m^2 [–]	$\sigma_{T_m}^2/\sigma_T^2$ [–]	T_0/T_X [–]
Southern Great Plains	3.43	12.4	0.36	0.06	0.49	0.66
Atlanta, GA	2.49	7.61	0.42	0.07	0.39	0.56
Wichita, KS	2.14	11.8	0.41	0.07	0.39	0.70
Dallas, TX	1.70	9.24	0.31	0.07	0.39	0.56
New York, NY	0.94	7.80	0.58	0.05	0.06	0.52

We use SMACM to derive a nonlinear Hasselmann-like model [31] for the VPD-driven soil moisture response to stochastic precipitation forcing. Again invoking slow timescales, we write

$$\mu \frac{dm}{dt} = \mathcal{P} - \nu\gamma T_0 \left(\frac{m}{1 + \eta m} \right). \tag{3}$$

(Derivation in *Methods*.) We see that η again determines the degree of nonlinearity. We show the distribution of soil moisture when (3) is forced with ERA5 precipitation time series in Figure 3A–C and see that our model largely reproduces the distribution of soil moisture found in ERA5, despite neglecting atmospheric forcing other than precipitation.

We use (3) to compute the ratio of temperature variance owing to soil moisture to total temperature variance in five locations in Table 2 (see *Methods* for calculation details). We find that in locations where η and T_0 are large, and soil moisture is generally dry while still maintaining non-negligible variance, the ratio of soil moisture induced temperature variance to total temperature variance is significant ($\gtrsim$ 40%). Meanwhile, New York has a low η and a relatively wet soil, leading to a small fraction of temperature variance owing to soil moisture. These findings corroborate the trends seen in Figure 1, where higher fractions of dry heat waves are found where the ratio of temperature variances seen in Table 2 are highest, and the lower fractions are found where variances are lowest.

Synthesis

We have explained soil moisture modulation of heat waves found in observations (see Fig. 1) by partitioning near-surface temperature fluctuations into a component driven by rapid atmospheric variability and another driven by slow soil moisture dynamics. We used a theoretical framework to encode these components into the fast and slow modes of a dynamical system. We find slow soil moisture variability has a nonlinear impact on the background temperature state, while rapid atmospheric variability is well-approximated as linearly additive on top of background state variations (Fig. 2G–L). The slow soil moisture variability itself is well approximated as primarily driven by stochastic precipitation, with other atmospheric forcing factors likely playing a secondary role (Fig. 3A–C).

Both a strong nonlinear coupling and significant soil moisture variability are required for soil moisture to be a strong control on heat waves. The degree of nonlinearity is encoded in the temperature nullcline (Eqn. (1)) and varies across space depending on land surface properties (such as the surface conductance and root-level soil moisture content). Differences in the strength of the nullcline partially explain the heterogeneity of soil moisture's influence on temperature extremes found in observations and in reanalysis. We quantified these differences in nullcline slope by introducing the coupling parameter η. In strongly coupled locales (where η is large), moisture depletion increases the potential for a heat wave, and atmospheric anomalies turn this potential into actuality. In weakly coupled locales (where η is small), soil moisture matters little for temperature extremes, as the nullcline "flattens out" and temperature extremes are determined primarily by atmospheric forcing.

By combining the nullcline (1) with the Hasselmann-like model for soil moisture (3), we can calculate the fraction of temperature variance attributable to soil moisture's influence on temperature. We find that the fraction of temperature variance attributable to soil moisture fluctuations is highest in the same locations where heat waves disproportionately favor dry soils (see Fig. 1). Over a majority of the continental midlatitude regions heat waves are conditioned on precipitation deficits depleting soil moisture and priming the surface for temperature extremes when a favorable atmospheric anomaly occurs.

Methods

Observational data

Daily temperature data are from the CPC Global Unified Temperature dataset, while daily soil moisture data are from the ESA-CCI v06.1 [32–34]. June, July, and August values of both quantities were used from 2010-2019. A value of 100 in Fig. 1a indicates that all days above the local 99$^{\text{th}}$ percentile occurred when the soil was drier than the local first quantile (i.e. all points above the orange line in Figs. 1b)–e) are also left of the green line).

Reanalysis data

ERA5 daily mean temperature and soil moisture data [28] for the southern great plains (we use the Department of Energy Atmospheric Radiation Measurement site for the precise coordinates for this analysis), Atlanta and New York are used to create Figure 2. In Figure 4, we use hourly precipitation and solar radiative forcing data from the SGP to force our model equations, as well as the climatological two meter dew point temperature.

Derivation of SMACM model equations

Consider a land surface with a dynamic temperature, T, and soil moisture content, m. m is a value between zero and unity that denotes the fractional saturation of the land surface. The land surface is coupled to a non-dynamic atmosphere with dew point temperature T_d and reference specific humidity q_r. In the energy sector, the land is forced by radiation from the Sun, denoted as $\mathcal{F}$. The surface cools by releasing heat through latent, sensible, and longwave channels. Thus, conservation of energy implies

$$C\frac{dT}{dt} = \mathcal{F} - F_{LW} - G - \mathcal{H} - \lambda\mathcal{E}, \tag{4}$$

where F_{LW} is the net longwave heat flux, G is the ground heat flux, $\mathcal{H}$ is the sensible heat flux, C is the effective surface heat capacity, λ is the latent heat of vaporization of water, and $\mathcal{E}$ is evapotranspiration. We parameterize the sum of the longwave, ground, and sensible heat fluxes as linear departures from the atmospheric dew point, such that

$$G + \mathcal{H} + F_{LW} = \alpha(T - T_d). \tag{5}$$

We parameterize evapotranspiration as,

$$\mathcal{E} = \nu m(q_s(T) - q_r), \tag{6}$$

where $q_s(T)$ is the saturation humidity given by the Clausius-Clapeyron relationship and ν is the surface evaporative conductance. Linearizing (6) around the dew point temperature yields

$$\mathcal{E} = \nu\gamma m(T - T_d), \tag{7}$$

where we have used that $q_s(T = T_d) = q_r$ and γ is the temperature derivative of the Clausius-Clapeyron relationship evaluated at the dew point temperature. Using (5) and (7) in (4) results in

$$C\frac{dT}{dt} = \mathcal{F} - (\alpha + \lambda\gamma\nu m)(T - T_d). \tag{8}$$

So far, this model is identical to the one presented in [19], but one final alteration is required to (8). Figure 4 shows that when the surface soil is depleted, the latent heat flux does not approach zero. This owes to the fact that deep, root-level soil moisture is present, and contributes to the latent heat flux. We therefore add an additional soil moisture fraction to (8) to capture this effect, denoted as m_0, resulting in the final temperature evolution equation,

$$C\frac{dT}{dt} = \mathcal{F} - (\alpha + \lambda\gamma\nu(m + m_0))(T - T_d), \tag{9}$$

as desired. Note that deep soil is assumed to act on longer timescales than are relevant for our analysis, and therefore is treated as constant.

In the moisture sector, we consider the conservation of water mass flux to write

$$\mu\frac{dm}{dt} = \mathcal{P} - \mathcal{E} - \mathcal{R} - \mathcal{I}, \tag{10}$$

where μ is the holding capacity of the soil, $\mathcal{P}$ is stochastic precipitation forcing, $\mathcal{R}$ is runoff and $\mathcal{I}$ is infiltration. In this model, runoff and infiltration act only to keep soil moisture within restricted bounds set by the field capacity, Θ; therefore, $\mathcal{R} = \mathcal{I} = 0$. At all other times, we have

$$\mu\frac{dm}{dt} = \mathcal{P} - \nu\gamma m(T - T_d), \tag{11}$$

Taken together, the governing equations of SMACM are

$$C\frac{dT}{dt} = \mathcal{F} - (\alpha + \lambda\gamma\nu(m + m_0))(T - T_d), \tag{12}$$

$$\mu\frac{dm}{dt} = \mathcal{P} - \nu\gamma m(T - T_d). \tag{13}$$

To derive the nullcline equation (1), we simply assume that the temperature derivative in (12) can be set to zero, owing to the assumption that the timescale of thermal adjustment is much smaller than that of soil moisture adjustment (as is evidenced by Fig. 2 as well as other studies, e.g., [18–20]). Setting (12) to zero and solving for T in terms of soil moisture results in (1) after some rearrangement of terms.

To derive the Hasselmann-like model for soil moisture, we use (1) for temperature in (13). Simplifying results in (3).

Model evaluation

We use reanalysis output from ERA5 1979–2021 over the SGP [28] to evaluate SMACM performance. Using hourly output for net shortwave radiation and precipitation as model forcings, taking T_d to be the average climatological two meter dew point temperature, and tuning the remaining free parameters, we arrive at the time series shown in Figure 4A–D. Of particular interest are periods where soil moisture is low (green shading in Figure 4), where a reduction in the latent heat flux (panel 4C) is met with an increase in the sensible and longwave heat fluxes (panel 4D), as well as an increase in near surface air temperature (panel 4A). Some high-frequency variability in SMACM is missing because we have not included fast fluctuations in atmospheric circulation;

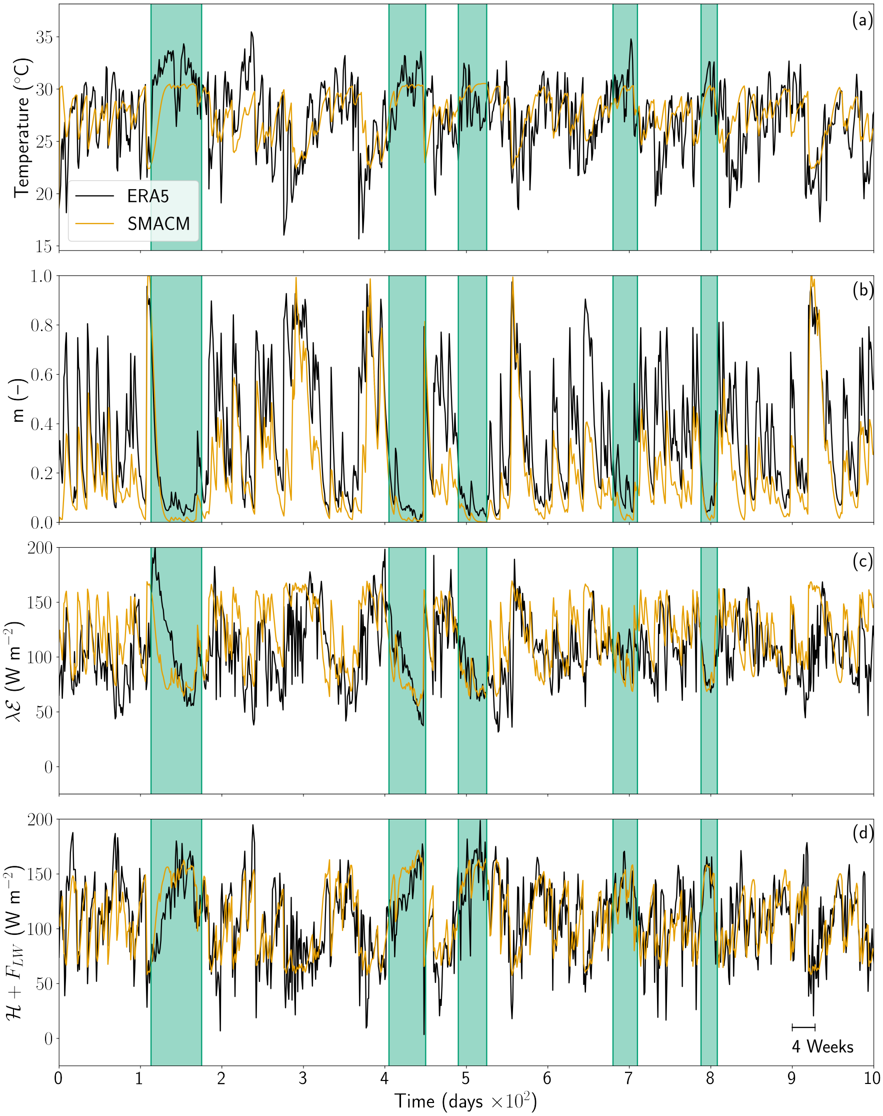

Fig. 4 Model evaluation. A comparison of SMACM to ERA5 output at the SGP. **A–D** show the near surface air temperature, soil moisture fraction, latent heat flux, and dry heat flux, respectively.

the only rapid fluctuations considered are fluctuations in shortwave radiation (the $\mathcal{F}$ term). Despite the lack of rapid atmospheric forcing, SMACM adequately reproduces soil moisture variations, as well as the partition of sensible and latent heat. SMACM is also able to reproduce slow variations in temperature, particularly elevated mean temperatures during times of dry soil moisture conditions.

Proof of timescale separation in SMACM

Throughout this paper, we have argued that all temperature variability can be decomposed into a "slow" mode driven by soil moisture fluctuations and a "fast" mode driven by fluctuations in shortwave radiation and thermal advection. Here we prove that, within SMACM, the timescale of thermal adjustment is fast relative to moisture adjustment, thus justifying our separation of timescales approach.

Assume in all that follows $\mathcal{P} = 0$, as we are analyzing the *response* of SMACM's model equations to precipitation forcing. Thus, the relevant equations are

$$\frac{dT}{dt} = \frac{1}{C}\left(\mathcal{F} - (\alpha + \lambda\gamma\nu(m + m_0))(T - T_d)\right) =: f_T(m, T), \tag{14}$$

$$\frac{dm}{dt} = -\frac{\nu\gamma m(T - T_d)}{\mu} =: f_m(m, T), \tag{15}$$

where we have defined the right-hand-sides of each equation for simplicity in what follows.

Step 1: Equilibrium analysis

The equilibria of (14)–(15) correspond to the set of solutions of the algebraic system $f_T(m, T) = f_m(m, T) = 0$. $f_m(m, T) = 0$ implies there are two equilibrium, namely $m = 0$ and $T = T_d$. However, $T = T_d$ does not satisfy the condition $f_T(m, T = T_d) = 0$ for any m, as $\mathcal{F} \neq 0$ by assumption and C is finite. Therefore, the sole equilibrium is given by $(m^*, T^*) = (0, T^*)$, where $T^* := \mathcal{F}/(\alpha + \lambda\nu\gamma m_0) + T_d$. This makes intuitive sense: the only equilibrium is a totally dry soil column, and the temperature is prescribed solely by atmospheric conditions and thermodynamic attributes of the surface.

Step 2: Determine stability of equilibrium

The stability of the equilibrium above is determined by the Jacobian of (14)–(15) [29]. Therefore, we evaluate

$$\mathcal{J}(m, T) = \begin{pmatrix} \partial_T f_T(m, T) & \partial_m f_T(m, T) \\ \partial_T f_m(m, T) & \partial_m f_m(m, T) \end{pmatrix}, \tag{16}$$

$$= \begin{pmatrix} -(\alpha + \lambda\nu\gamma(m + m_0))/C & -\lambda\nu\gamma(T - T_d)/C \\ -\nu\gamma m/\mu & -\nu\gamma(T - T_d)/\mu \end{pmatrix}, \tag{17}$$

where $\partial_x := \partial/\partial x$. Evaluating (17) at (m^*, T^*) results in

$$\mathcal{J}(m^*, T^*) = \begin{pmatrix} -(\alpha + \lambda\nu\gamma m_0)/C & -\lambda\nu\gamma\mathcal{F}/(C(\alpha + \lambda\nu\gamma m_0)) \\ 0 & -\nu\gamma\mathcal{F}/(\mu(\alpha + \lambda\nu\gamma m_0)) \end{pmatrix}. \tag{18}$$

Equation (18) is an upper triangular matrix, and therefore the eigenvalues lie on the diagonals, and the corresponding eigenvectors are the columns [35]. Therefore, the eigenvalues are,

$$E_1 := -\frac{\alpha + \lambda\nu\gamma m_0}{C}, \qquad E_2 := -\frac{\nu\gamma\mathcal{F}}{\mu(\alpha + \lambda\nu\gamma m_0)}. \tag{19}$$

As both eigenvalues are negative, the equilibrium (m^*, T^*) is a stable node [29].

Step 3: Solve for eigenvectors

As mentioned above, the eigenvectors are the columns of (18). Therefore, we have

$$\vec{\xi}_1 := \begin{pmatrix} 1 \\ 0 \end{pmatrix}, \qquad \vec{\xi}_2 := \begin{pmatrix} \dfrac{\mathcal{F}\lambda\nu\gamma\mu}{C\mathcal{F}\nu\gamma - (\alpha + \lambda\nu\gamma m_0)^2\mu} \\ 1 \end{pmatrix}, \tag{20}$$

where we've simplified each eigenvector to illustrate the point that $\vec{\xi}_1$ points solely along the T-axis, and therefore corresponds to thermal adjustments only. It follows that the timescale associated along this direction of decay corresponds to the timescale of thermal adjustment, whereas the timescale of decay along $\vec{\xi}_2$ corresponds to moisture adjustment (and the resulting temperature adjustment as the soil dries). This proves that temperature has two modes that evolve on different timescales, as represented in (1)).

Step 4: Compare timescales of decay

The timescales of decay along $\vec{\xi}_1$ and $\vec{\xi}_2$ are found by taking the absolute value and inverse of their corresponding eigenvalues [29], such that

$$\tau_1 = \frac{C}{\alpha + \lambda\nu\gamma m_0}, \qquad \tau_2 = \frac{\mu(\alpha + \lambda\nu\gamma m_0)}{\nu\gamma\mathcal{F}}. \tag{21}$$

Using the average order of magnitude of each parameter from Table 1, we find that,

$$\frac{\tau_2}{\tau_1} \sim 10^6. \tag{22}$$

Thus, we have shown that the timescale of purely thermal adjustment, τ_1, is fast relative to the timescale of moisture adjustment and its influence on temperature, τ_2, as desired.

Calculation the temperature variance owing to soil moisture

To calculate the ratios of temperature variance owing to soil moisture to dew point temperature variance, we utilize the ERA5 soil moisture time series at each location and use it to force (1). The variance is then taken, and compared with the dew point temperature variance from ERA5 in each location. The parameter values at each location (i.e., η and T_0) are calculated by fitting the model to ERA5 time series, as was done in Figure 4. Soil moisture mean and variance is calculated from ERA5.

References

[1] García-León, D., Casanueva, A., Standardi, G., Burgstall, A., Flouris, A.D., Nybo, L.: Current and projected regional economic impacts of heatwaves in Europe. Nature Communications **12**(1), 5807 (2021). https://doi.org/10.1038/s41467-021-26050-z. Accessed 2021-12-22

[2] Sippel, S., Zscheischler, J., Reichstein, M.: Ecosystem impacts of climate extremes crucially depend on the timing. Proceedings of the National Academy of Sciences **113**(21), 5768–5770 (2016) https://www.pnas.org/doi/pdf/10.1073/pnas.1605667113. https://doi.org/10.1073/pnas.1605667113

[3] Robine, J.-M., Cheung, S.L.K., Le Roy, S., Van Oyen, H., Griffiths, C., Michel, J.-P., Herrmann, F.R.: Death toll exceeded 70,000 in Europe during the summer of 2003. Comptes Rendus Biologies **331**(2), 171–178 (2008). https://doi.org/10.1016/j.crvi.2007.12.001. Dossier : Nouveautés en cancérogenèse / New developments in carcinogenesis

[4] IPCC: Climate change 2021: The physical science basis (2021)

[5] Rhines, A., Huybers, P.: Frequent summer temperature extremes reflect changes in the mean, not the variance. Proceedings of the National Academy of Sciences **110**(7) (2013). https://doi.org/10.1073/pnas.1218748110. Accessed 2022-09-20

[6] Huybers, P., McKinnon, K.A., Rhines, A., Tingley, M.: U.S. Daily Temperatures: The Meaning of Extremes in the Context of Nonnormality. Journal of Climate **27**(19), 7368–7384 (2014). https://doi.org/10.1175/JCLI-D-14-00216.1. Accessed 2022-09-20

[7] Philip, S.Y., Kew, S.F., van Oldenborgh, G.J., Anslow, F.S., Seneviratne, S.I., Vautard, R., Coumou, D., Ebi, K.L., Arrighi, J., Singh, R., van Aalst, M., Pereira Marghidan, C., Wehner, M., Yang, W., Li, S., Schumacher, D.L., Hauser, M., Bonnet, R., Luu, L.N., Lehner, F., Gillett, N., Tradowsky, J., Vecchi, G.A., Rodell, C., Stull, R.B., Howard, R., Otto, F.E.L.: Rapid attribution analysis of the extraordinary heatwave on the pacific coast of the US and Canada june 2021. Earth System Dynamics Discussions **2021**, 1–34 (2021). https://doi.org/10.5194/esd-2021-90

[8] Chan, D., Rigden, A., Proctor, J., Chan, P.W., Huybers, P.: Differences in Radiative Forcing, Not Sensitivity, Explain Differences in Summertime Land Temperature Variance Change Between CMIP5 and CMIP6. Earth's

Future **10**(2) (2022). https://doi.org/10.1029/2021EF002402. Accessed 2022-09-26

[9] Zeppetello, L.R.V., Battisti, D.S.: Projected Increases in Monthly Midlatitude Summertime Temperature Variance Over Land Are Driven by Local Thermodynamics. Geophysical Research Letters **47**(19) (2020). https://doi.org/10.1029/2020GL090197. Accessed 2020-12-04

[10] Byrne, M.P.: Amplified warming of extreme temperatures over tropical land. Nature Geoscience **14**(11), 837–841 (2021). https://doi.org/10.1038/s41561-021-00828-8. Accessed 2021-12-22

[11] Zhang, Y., Held, I., Fueglistaler, S.: Projections of tropical heat stress constrained by atmospheric dynamics. Nature Geoscience **14**(3), 133–137 (2021). https://doi.org/10.1038/s41561-021-00695-3. Accessed 2022-12-02

[12] Pfahl, S., Wernli, H.: Quantifying the relevance of atmospheric blocking for co-located temperature extremes in the northern hemisphere on (sub-)daily time scales. Geophysical Research Letters **39**(12) (2012)

[13] Meehl, G.A., Tebaldi, C.: More Intense, More Frequent, and Longer Lasting Heat Waves in the 21st Century. Science **305**(5686), 994–997 (2004). https://doi.org/10.1126/science.1098704. Accessed 2021-12-22

[14] Schneider, T., Bischoff, T., Płotka, H.: Physics of Changes in Synoptic Midlatitude Temperature Variability. Journal of Climate **28**(6), 2312–2331 (2015). https://doi.org/10.1175/JCLI-D-14-00632.1. Accessed 2021-12-22

[15] Tamarin-Brodsky, T., Hodges, K., Hoskins, B.J., Shepherd, T.G.: Changes in Northern Hemisphere temperature variability shaped by regional warming patterns. Nature Geoscience **13**(6), 414–421 (2020). https://doi.org/10.1038/s41561-020-0576-3. Accessed 2021-01-06

[16] Lorenz, R., Jaeger, E.B., Seneviratne, S.I.: Persistence of heat waves and its link to soil moisture memory. Geophysical Research Letters **37**(9), (2010). https://doi.org/10.1029/2010GL042764. Accessed 2021-11-13

[17] Vargas Zeppetello, L.R., Battisti, D.S.: Projected increases in monthly midlatitude summertime temperature variance over land are driven by local thermodynamics. Geophysical Research Letters **47**(19), 2020–090197 (2020). https://doi.org/10.1029/2020GL090197

[18] Seneviratne, S.I., Koster, R.D., Guo, Z., Dirmeyer, P.A., Kowalczyk, E., Lawrence, D., Liu, P., Mocko, D., Lu, C.-H., Oleson, K.W., Verseghy, D.: Soil Moisture Memory in AGCM Simulations: Analysis of

Global Land–Atmosphere Coupling Experiment (GLACE) Data. Journal of Hydrometeorology **7**(5), 1090–1112 (2006). https://doi.org/10.1175/JHM533.1. Accessed 2021-12-22

[19] Vargas Zeppetello, L.R., Battisti, D.S., Baker, M.B.: The physics of heat waves: What causes extremely high summertime temperatures? Journal of Climate **35**(7), 2231–2251. https://doi.org/10.1175/JCLI-D-21-0236.1. Accessed 2022-07-20

[20] Koster, R.D., Suarez, M.J.: Soil Moisture Memory in Climate Models. Journal of Hydrometeorology **2**(6), 558–570 (2001). https://doi.org/10.1175/1525-7541(2001)002⟨0558:SMMICM⟩2.0.CO;2. Accessed 2021-12-22

[21] Proistosescu, C., Rhines, A., Huybers, P.: Identification and interpretation of nonnormality in atmospheric time series. Geophysical Research Letters **43**(10), 5425–5434 (2016). https://doi.org/10.1002/2016GL068880. Accessed 2021-01-11

[22] Schumacher, D.L., Keune, J., van Heerwaarden, C.C., Vilà-Guerau de Arellano, J., Teuling, A.J., Miralles, D.G.: Amplification of mega-heatwaves through heat torrents fuelled by upwind drought. Nature Geoscience **12**(9), 712–717 (2019). https://doi.org/10.1038/s41561-019-0431-6. Accessed 2022-09-27

[23] Bieli, M., Pfahl, S., Wernli, H.: A Lagrangian investigation of hot and cold temperature extremes in Europe: Lagrangian Investigation of Hot and Cold Extremes. Quarterly Journal of the Royal Meteorological Society **141**(686), 98–108 (2015). https://doi.org/10.1002/qj.2339. Accessed 2022-09-27

[24] Budyko, M.I.: The Heat Balance of the Earth's Surface. Soviet Geography **2**(4), 3–13 (1961). https://doi.org/10.1080/00385417.1961.10770761. Accessed 2022-09-28

[25] Manabe, S.: Climate and the Ocean Circulation: I. The Atmospheric Circulation and the Hydrology of the Earth's Surface. Monthly Weather Review **97**(11), 739–774 (1969). https://doi.org/10.1175/1520-0493(1969)097⟨0739:CATOC⟩2.3.CO;2. Accessed 2021-12-22

[26] Sellers, P.J., Dickinson, R.E., Randall, D.A., Betts, A.K., Hall, F.G., Berry, J.A., Collatz, G.J., Denning, A.S., Mooney, H.A., Nobre, C.A., Sato, N., Field, C.B., Henderson-Sellers, A.: Modeling the Exchanges of Energy, Water, and Carbon Between Continents and the Atmosphere. Science **275**(5299), 502–509 (1997). https://doi.org/10.1126/science.275.5299.502. Accessed 2022-09-28

[27] Whan, K., Zscheischler, J., Orth, R., Shongwe, M., Rahimi, M., Asare, E.O., Seneviratne, S.I.: Impact of soil moisture on extreme maximum temperatures in Europe. Weather and Climate Extremes **9**, 57–67 (2015). https://doi.org/10.1016/j.wace.2015.05.001. Accessed 2022-09-28

[28] Copernicus Climate Change Service: ERA5-Land monthly averaged data from 2001 to present. ECMWF. Type: dataset (2019). https://doi.org/10.24381/CDS.68D2BB30. https://cds.climate.copernicus.eu/doi/10.24381/cds.68d2bb30 Accessed 2021-12-20

[29] Strogatz, S.H.: Nonlinear Dynamics and Chaos vol. 1, 2nd edn. Westview Press, Boulder, CO (2018)

[30] Bauer, A., Carter, P.: Existence of Transonic Solutions in the Stellar Wind Problem with Viscosity and Heat Conduction. SIAM Journal on Applied Dynamical Systems **20**(1), 262–298 (2021). https://doi.org/10.1137/20M1314240. Accessed 2021-12-16

[31] Hasselmann, K.: Stochastic climate models Part I. Theory. Tellus **28**(6), 473–485 (1976). https://doi.org/10.1111/j.2153-3490.1976.tb00696.x. Accessed 2021-01-11

[32] Gruber, A., Scanlon, T., van der Schalie, R., Wagner, W., Dorigo, W.: Evolution of the esa cci soil moisture climate data records and their underlying merging methodology. Earth System Science Data **11**(2), 717–739 (2019). https://doi.org/10.5194/essd-11-717-2019

[33] Dorigo, W., Wagner, W., Albergel, C., Albrecht, F., Balsamo, G., Brocca, L., Chung, D., Ertl, M., Forkel, M., Gruber, A., Haas, E., Hamer, P.D., Hirschi, M., Ikonen, J., de Jeu, R., Kidd, R., Lahoz, W., Liu, Y.Y., Miralles, D., Mistelbauer, T., Nicolai-Shaw, N., Parinussa, R., Pratola, C., Reimer, C., van der Schalie, R., Seneviratne, S.I., Smolander, T., Lecomte, P.: ESA CCI soil moisture for improved earth system understanding: State-of-the art and future directions. Remote Sensing of Environment **203**, 185–215 (2017). https://doi.org/10.1016/j.rse.2017.07.001. Earth Observation of Essential Climate Variables

[34] Gruber, A., Dorigo, W.A., Crow, W., Wagner, W.: Triple Collocation-Based Merging of Satellite Soil Moisture Retrievals. IEEE Transactions on Geoscience and Remote Sensing **55**(12), 6780–6792 (2017). https://doi.org/10.1109/TGRS.2017.2734070. Accessed 2022-07-27

[35] Axler, S.J.: Linear Algebra Done Right. Undergraduate Texts in Mathematics. Springer, New York (1997). http://linear.axler.net/

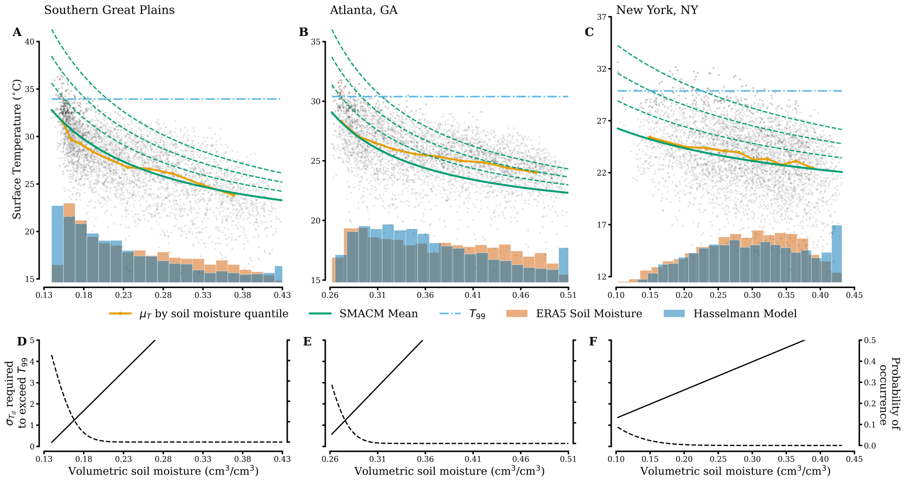

Fig. 5 As Figure 3, but with anomalies being applied in the radiative forcing, $\mathcal{F}$, rather than dew point temperature.

Supplementary information.

Acknowledgments. CPC Global Unified Temperature data provided by the NOAA PSL, Boulder, Colorado, USA, from their website. The authors thank Yi Zhang, David Battisti, Karen McKinnon, Peter Huybers, and the Huybers research group at Harvard University for helpful discussions related to this work. AMB is supported by a National Science Foundation Graduate Research Fellowship grant No. DGE 21-46756. LRVZ is supported by the James S. McDonnell Foundation and the Harvard University Center for the Environment. Computations were performed on the Keeling computing cluster, a computing resource operated by the School of Earth, Society and the Environment (SESE) at the University of Illinois at Urbana Champaign.

Competing interests. The authors declare no competing interests.

Author contributions. AMB carried out research tasks, did analytic calculations, and prepared figures. LRVZ created Figure 1. CP contributed to Figure 2. LRVZ and CP provided advising and designed the project. AMB, LRVZ, and CP wrote the manuscript.